



PERFORMANCE EVALUATION OF BISMUTH TELLURIDE SEMICONDUCTOR BASED PARABOLIC DISH CONCENTRATED SOLAR THERMOELECTRIC GENERATOR IN REALISTIC METEOROLOGICAL CONDITIONS OF CENTRAL INDIA

Sanjeev Kumar Bhukesh^{1,*}, Anil Kumar² and Suresh Kumar Gawre³

¹Energy Centre, Maulana Azad National Institute of Technology, Bhopal -462003
(India)

²Dept. of Mechanical Engineering, Delhi Technological University, Delhi-110 042 (India)

³Dept. of Electrical Engineering, Maulana Azad National Institute of Technology Bhopal-
462003 (India)

Abstract

Maintaining desired temperature difference between hot and cold sides (ΔT) in thermoelectric generator without harming environment, with feasible cost is a greater challenge. In this research an attempt has been made to maintain ΔT within a certain limit by means of DC fan air cooling which is powered by TEG itself. A 10W Bi_2Te_3 semiconductor based thermoelectric generator is fabricated where heat input is received from solar parabolic dish concentrator. Various operating parameters such as Global radiation, concentrated radiation, diffuse radiation, ambient temperature, hot and cold side temperature, ambient air velocity, ambient relative humidity, voltage and current are observed after regular interval of time. Max. hot side temperature 210°C , cold side temperature 45°C , TEG output voltage of 10V instead of 12V (rated), TEG output current of 0.694 A instead of rated current 1 A at a beam radiation of 726 W/m^2 are observed. Maximum electrical TEG power output was calculated $\approx 7 \text{ W}$ instead of rated power 10 W. Experimental observations are used for performance evaluation of developed TEG in terms overall system efficiency. The overall Parabolic dish concentrated solar thermoelectric generator PDCSTEG system efficiency are determined as 0.6207%. Concentrated solar power integrated TEG is a feasible renewable power solution.

Keywords: Thermoelectric Generator; Solar Power; temperature difference; Overall efficiency

1. Introduction

Population explosion and industrial growth has raised a need to examine various renewable energy resources. Globally 6 major **Global Horizontal Irradiation (GHI)** hotspots are identified (Australia, the Arabian Peninsula, Southern, Northern, Eastern and South Western Africa, Western South America) having rich value of $>2200 \text{ kWh/m}^2$ annually and 6 major **Direct Normal Irradiation (DNI)** hotspots as (Australia, Tibetan Plateau, North Western Arabian Peninsula, South Western Africa, Western South America, South Western North America) having potential of $>2500 \text{ kWh/m}^2$ [1]. India is blessed with 300 sun shine days per year, irradiation of $4\text{-}7 \text{ kWh/m}^2/\text{day}$ and across the country between 2300 and 3200 sunshine hours. National Institute of Solar Energy, India (NISE) admits India's solar power potential

around 750 GW [2]. The largest SPV plant (750 MW) has been approved by the state government of Madhya Pradesh, India. By the year 2022, India is committed to achieve its renewable energy target of 220 GW out of which 100 GW would be contributed by the solar power which was earlier 20 GW [3]. Nowadays most of the solar energy is harnessed through photovoltaic systems which deal with the direct conversion of incoming solar radiation into electrical energy using solar cells. The efficiency of solar cells is not very high (usually $\leq 20\%$) and demand large area of land [4]. **Thermo-Electric Generator (TEG)** is a solid state robust device that converts heat from various sources into useful electric power and has gained popularity among researcher and renewable energy stakeholders in the energy market. Solid state device nature, absence of moving part, operable at high temperature and stability in harsh environment due to its robustness are the features of this technology that suits for standalone power conversion or in hybrid solar thermal-electrical power systems. TEG integrated with parabolic dish forms PDCSTEG that harnesses solar energy from sun through concentrating solar power (CSP) technology. Concentrated radiations gets convert into heat to drive TEG [4], [5].

TE power generation mechanism converts directly heat into electric power via Seebeck effect. A electrical potential difference is generated between two junctions of two dissimilar material conductors and semiconductors due to temperature difference between the two junctions [6].

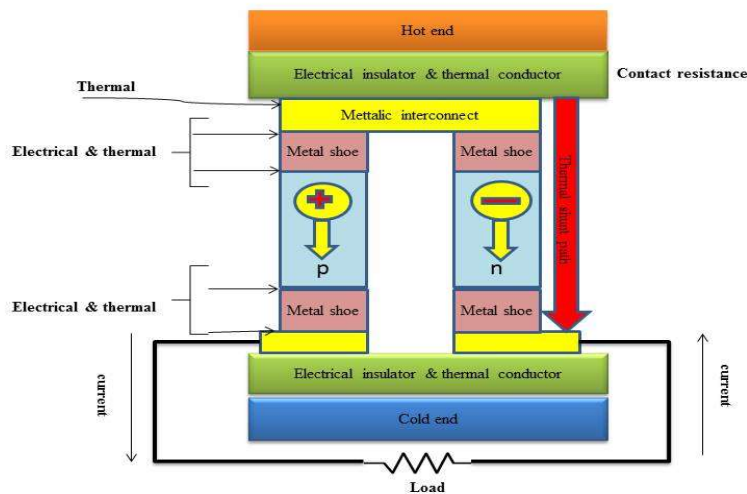


Figure 1.

Electrical and thermal interfaces in the architecture of a single p-n leg of a TEG [7]

A large number of p-type and n-type TE elements connected alternately electrically in series and thermally in parallel in a TEG module [7]. **Energy** efficient TEGs need to be fabricated with a high performance TE material, high figure of merit, higher temperature difference ΔT and with the ability of efficiently recovery of waste heat from various heat sources [7], [8]. Metal based, semiconductor based, ceramic based and polymer based TE materials are recommended for wide range of figure of merit (ZT) [9]. TEG operate at various operating temperature in the range 250-650 °C with high figure of merit TE material ZT of >2 by enhancing the power factor and reducing thermal conductivity [7]. In a PDCSTEG system, concentrated solar radiation

absorption increases at receiver, which ultimately results increased temperature gradient across TEG device [4]. There are two main approaches of increasing the temperature difference in PDCSTEG: (i) optical concentration enhancement of sunlight to increase the heat flux at the absorber surface, and (ii) increase thermal concentration, which means larger area of highly thermally conducting absorber than the area of the TE legs, allowing increased heat flux through the legs. Latter approach demonstrates STEG efficiencies of 4.6% and 5.2% with light intensities corresponding to 1 kW/m² and 1.5 kW/m² respectively [8]. The maximum output power and TE conversion efficiency also depends on an optimal length ratio of the segmented TE leg. This ratio does not only depend on the TE properties of the material but also on geometry and heat transfer conditions [10]. By improving TE leg with the help of segmented TE material and using high-temperature (600°C) spectrally selective solar absorber, thereby combining optical and thermal concentration, at an optically concentrated normal solar irradiance of 211 kW/m². **Chen et al.** investigated CSTEGs with a peak efficiency of 9.6% and 7.4% after considering optical concentration losses [5]. Length of the TE leg affects the optimized shape parameter, if contact resistance is taken into account [11]. By keeping element length constant, reducing the cross-sectional area of TE element and increasing the substrate area, thermal concentration increases that lead to efficiency improvement [5], [12]. Through desired geometry optimization of TE leg, TEG performance in terms of output power and efficiency can be improved and having constant cross section area of TE leg maximum output power per unit mass can be achieved for an ideal ATEG. Protic and Aprotic Ionic liquid TE cell based TEG sandwiched between a heated and a cooled electrode, which works in the range of room temperature and 300°C, exhibit temperature-dependent current, voltage and power output characterization [13]. The maximum efficiency also depends upon number of TEG modules integrated in an assembly. **Kurt** used the performance data of a full one year cycle solar irradiation to optimize the number of commercial TEGs for heat to electricity conversion in CSTEG [14]. It was observed that with an assembly of less TEGs, high concentration ratio and high temperature difference is achieved with more electric power as compared to an assembly of more number of TEGs [15]. Light spectrum is also responsible for improved efficiency of TEG. UV and visible solar spectrum energy is converted by photovoltaic, and IR spectrum energy can be utilized by thermo-electrics. The utilized spectrum range can be extended by combining and optimizing PV and TE hybrid system, hence improved efficiency can be achieved [15]. The structure, area and receiver material are also determinants of efficiency of a TEG. Fem to second laser irradiation creates an nano-structure surface on Al receiver that enhances absorption of UV and visible spectrum with small emissivity in infrared. Power generating capacity and efficiency of STEG integrated with Al foil receiver increased significantly [16]. Semiconductor based multilayer selective absorber could be an appropriate option for non-concentrated sunlight which shows low emissivity in the thermal wavelength range and high absorptivity for the visible solar spectrum. Therefore, solar concentrators can be avoided for medium temperature solar applications [17]. The highest efficiency ever reported by TEG is 15% across $T_h - T_c = 1000 - 200^\circ\text{C}$ by combining several next generation TE material. High flux solar furnace and selective solar absorber are used to achieve TEG efficiency greater than 15% [8]. Hollaran determines the power and efficiency of a commercial TEG with the help of LabVIEW data acquisition system [18]. **Chen et al.** investigated the performance of a TEG under the influence of sinusoidal temperature distribution at the hot side

or cold side surface[19]. TEG performance is not affected by the time period of temperature oscillations. Increase in concentration ratio increases the efficiency of PDCSTEG [20]. Various concentrating technologies have been used to harness the solar energy like, A solar tracker based on mosaic set of mirrors integrated with Bi_2Te_3 based CSTEG with running water cooling achieve hot side temperature of 200°C and the cold side temperature 50°C , produces 20W of electrical energy and 200W of thermal energy stored in water with a temperature of 50°C [21].**Date et al.** developed a Fresnel lens (heat flux 50000 W/m^2) based CSTEG with solar water heating. Heat pipe condenser immersed in water tank passively cool the cold side with a higher heat transfer coefficient[22].Heat source like phase change material, geothermal heat or solar pond (low-grade heat source) show continuity for thermal-electrical energy conversion therefore suitable for TE power generation investigated [21]. PCM based R- STEG provides 60% and 86% higher peak energy conversion efficiency for solar irradiance of 1 kW m^{-2} and 1.5 kW/m^2 as compared to typical STEG, therefore PCM can help to generate steady electrical energy [23].

For the evaluation of prototype CSTEG **PENG LI et al.**[20]developed a discrete numerical model by dividing TE leg into finite elements and considered temperature dependence of the TE material properties, achieved improved conversion efficiency for higher temperature gradient with increase in concentration ratio. **Tobereret al.**[24]developed a novel detailed balance model for CSTEG and applied this model for an incident flux 100 kW/m^2 and $T_h - 1000^\circ\text{C}$ and ensure 15.9% efficiency and with $ZT = 2$, 30.6%.**Manikandan et al** developed and analysed an irreversible and exoreversible thermodynamic model of the combined TEG-TEC compatible system in MATLAB environment with consideration of temperature dependent TE properties and with maximum power point tracker[25].Seebeck effect, modelling of TE phenomenon and TEG system geometry is investigated through an ANSYS computer program that involves modelling of complicated geometry of real objects, application of differentiable or discontinuous functions, which enable description of physical parameters and boundary conditions through finite element method (FEM). It reveals that increasing ΔT between hot and cold reservoir leads to produce higher voltage and electric power[26]. By means of ANSYS, the finite element analysis (FEA) was conducted on a model of the solar waste heat recovery based TEG attached with Al plate on the hot side. If area and thickness of the Al plate increased, the temperature gradient between hot and cold sides of TEG increases because of the increase in thermal resistance of Al plate. Thereby voltage produced gets increased [27]. By developing a Simulink model and thermal concentration optimization in realistic terrestrial environment for CSTEG, It was observed that thermal concentration in realistic environment gets doubled as compared to standard test condition[19]. A thermodynamic model for a CSTEG was developed and optimized in MATLAB environment. For maximum energy efficiency of 5.85% and maximum exergy efficiency of 6.29% optimized concentration ratio is achieved as 180 and load resistance ratio as 1.3 respectively, with corresponding power output of 4.213W [28]. An equivalent model based on 3-dimensional finite element scheme advocates that the thermal concentration ratio gets increased by keeping element length constant, reducing the cross-sectional area of TE element and increasing the substrate area that leads to improvement in efficiency and performance of CSTEG[12].**Q. Cao et al.** developed a generalised model for investigating various effects of geometry configuration and contact resistance of an annular TEG[11]. Desired optimization of TE leg led to improve the performance of TEG in terms of

output power. In a Solar heat pipe based cylindrical annular TEG (SATEG) the thermal energy output and thermal exergy efficiency with overall exergy efficiency of SATEG are found little bit lower than that of the SFTEG, however with the higher FOM TE materials, SATEG will gain its importance in near future [29].

The solar heat pipe/thermoelectric hybrid system in which the TE modules combined with solar heat pipe provide an ultimate device for simultaneous electricity generation [30]. A concentrating photovoltaic/thermoelectric hybrid generator was developed by T.H Kil et al. consisting of single-junction GaAs-based solar cell and a conventional TE module and achieved a 3% higher efficiency as compared to the single CPV cell at the solar concentration of 50 suns [31]. Typical applications of the solar-driven thermoelectric refrigeration and the solar-driven TE power generation are presented [32]. It is an estimation of scientists and researchers that almost 70% of world energy is wasted in the form of heat to the atmosphere and led to a major factor in global warming [4]. TEGs have potential to harvest the heat of human body and waste heat from various sources [33], [34].

Therefore, heat generated from CSP technology and waste heat from various sources can be utilized by TEG in more efficient way. Small scale power generation confines the area of receiver plate, due to which complexity in design of small scale power generating PDCSTEG system gets increased, if CSP technology is employed. In this research to examine a TEG sandwiched between aluminium receiver plate (without any selective absorber coating) and aluminium heat sink integrated with solar parabolic dish concentrator at Energy centre (Bhopal City 23° 16'N, 77° 36'E), a trade of between the concentrator aperture area and the absorber plate has been set which keeps ΔT within specified range. For central India it is a very first kind of study of performance of concentrated solar thermoelectric generator which could help to provide renewable power solution for Indian villages.

2. Materials and Methods

2.1. Experimental Setup of PDCSTEG System

The arrangement of solar parabolic dish thermoelectric generator is shown in **Figure 2**. A parabolic dish concentrator is integrated with a set of two thermoelectric modules (each 5 watt) connected in series, sandwiched between uncovered flat plate aluminium solar thermal absorber/receiver (hot side) and aluminium air cooled heat sink (cold side) and hence a PDCSTEG is so constructed. The TEG set is placed on a focal plane of solar PDC.

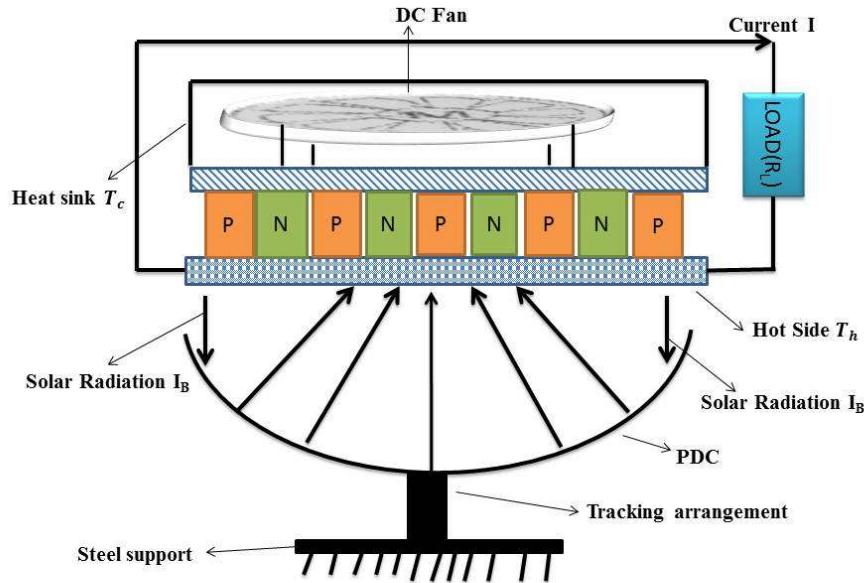


Figure 2. Arrangement of PDCSTEG

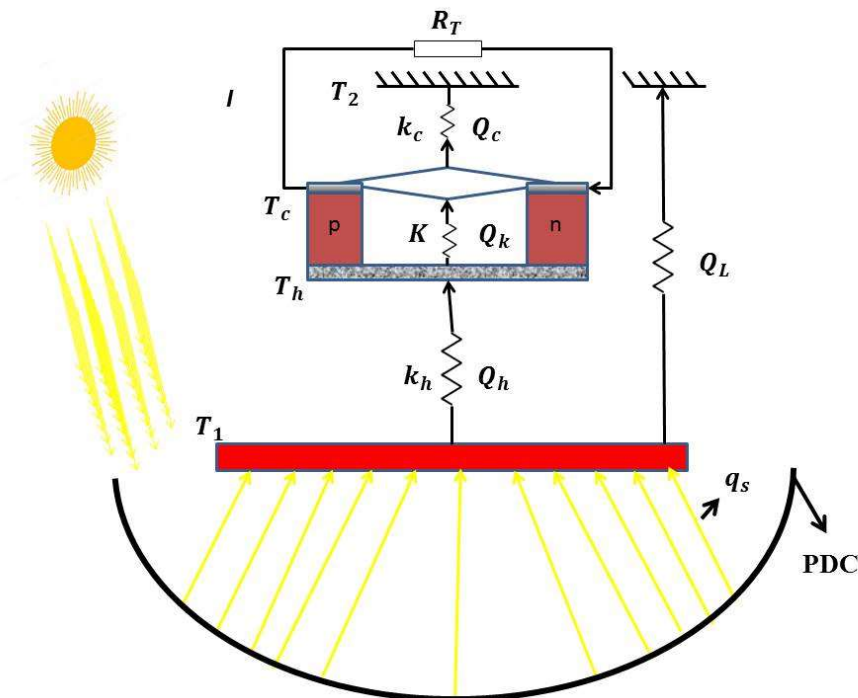


Figure 3. Heat transfer in a PDCSTEG

2.2. Various tests on PDCSTEG

The complete experimental setup was installed in the yard area of the Energy Centre, Maulana Azad National Institute of Technology Bhopal (Latitude: $23^{\circ} 16'N$, Longitude: $77^{\circ} 36'E$), India. Photographs of the experimental set up are shown in **Figure 4**. The focal point of the solar PDC is the position where the absorber/receiver plate is positioned. Sun is tracked

manually with one axis rotation of the dish. Dish parameters are measured as open mouth diameter of 1.4 m, focus of 0.285 m, height of 0.43 m and aperture angle of 101.7° . For absorption of solar concentrated radiation from PDC, two TE modules (each 5watt) connected in series are sandwiched between the hot side of receiver and heat sink. For testing purpose the TE modules are loaded with an electrical Resistance of 16.94Ω in accordance with the maximum power transfer theorem. Mass flow rate of fan's air tries to maintain the cold side temperature at $35-43^{\circ}\text{C}$.

Table 1. Air velocity and Relative humidity Variation with time

Parameter	Min Value at 1430 hrs	Max Value at 1300 hrs	Value at 1100 hrs	Value at 1400 hrs
Ambient air velocity V_a	0.13 m/s	1.20 m/s	0.85 m/s	0.18 m/s
Relative humidity Rh_a	12.1% at 1615 hrs	30.1% at 800 hrs	21.2%	14.2%.

The best performance analysis time duration is between 1100 hrs to 1400 hrs as shown in table 1. The maximum value and minimum value of both the parameter are very effective parameter to affect the temperature gradient and ultimately the power generated.

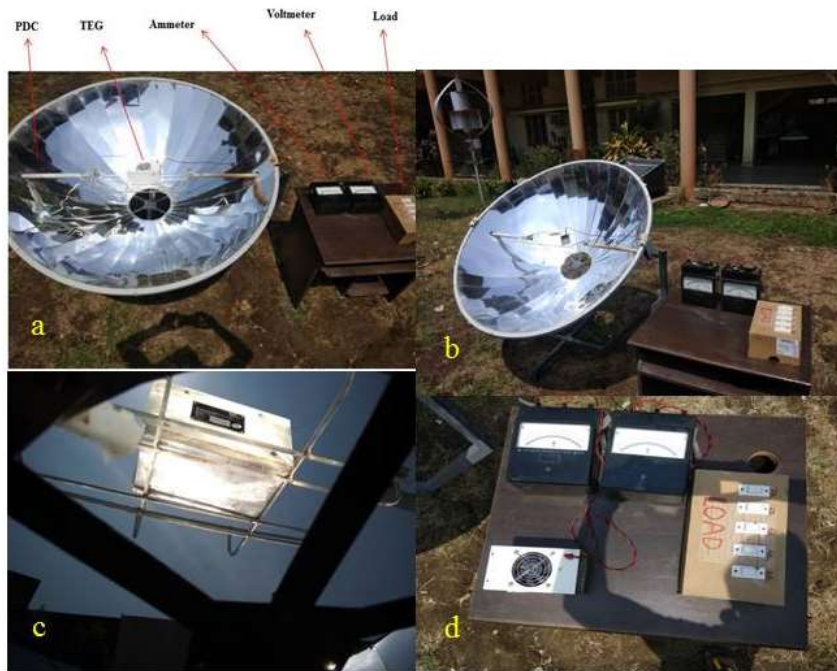


Figure 4.(a)- Top view of PDCSTEG(b) Side view of PDCSTEG(c) Focused concentrated radiation(d) TEG, Load Box, Ammeter, Voltmeter

2.2.1. No Load Test/Open Circuit Test

The first test conducted on the PDCSTEG was an open circuit test in the yard of Energy Centre, by connecting the module output wires to a DC voltmeter as shown in **Figure 5**. open circuit voltage can be measured. The sun was tracked manually throughout the day from 800 hrs to

1645 hrs. Observations were recorded at each 15 minutes interval. The open circuit voltage was also recorded for given time intervals until it reaches at steady-state. The constant input solar power was recorded using a solar power meter, made by Ambient Weather. The open circuit voltage varies between 6.1volts(min) to 9.5volts(max) during 1100 hrs and 1400 hrs.

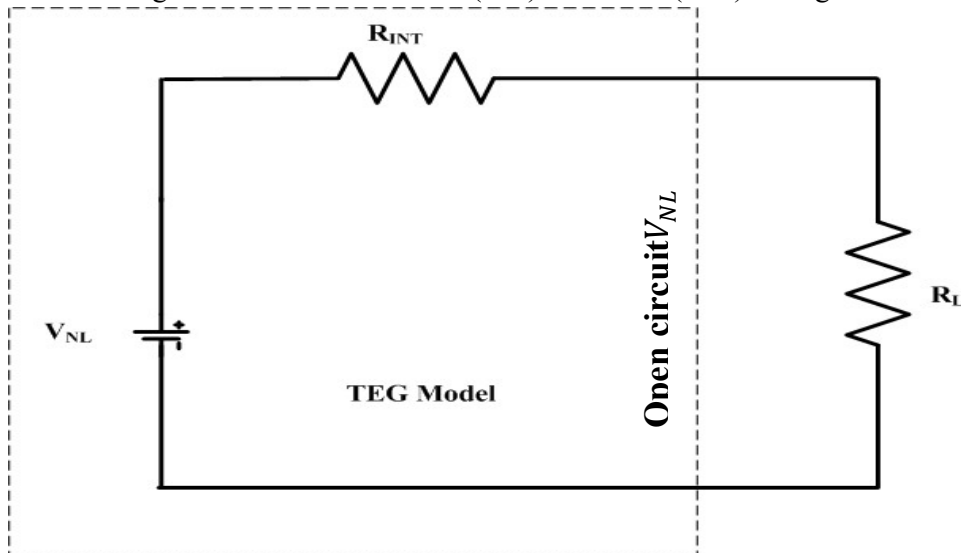


Figure 5. Circuit diagram of a TEG model

2.2.2. Loaded Tests

For the load test of the PDCSTEG, the TEG assembly was first placed at the focus of solar PDC where maximum concentrated radiations were received. The device is kept for about an hour to allow the entire device to reach ambient temperature. When the PDCSTEG was moved into the sun, the solar power input (Beam radiation) and output voltage were measured at every 15 minute from 800 hrs to 1645 hrs on 4th May 2021. A decade box was connected to the output wires of the module as the resistive load and a DC voltmeter is connected across the load and ammeter is connected in series with R_T . The test is conducted for: 1-Fan load (96Ω) 2- Half load ($R_T = 28.28 \Omega$) 3-Full load $R_T = 14.4 \Omega$. ($R_T = R_{FAN} \parallel R_L$) as shown in **Figure 6**.

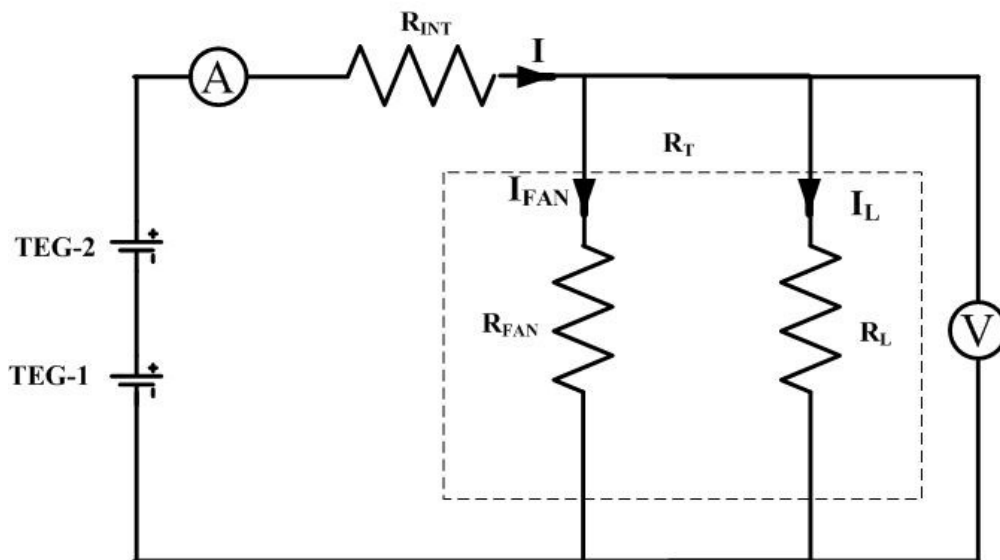


Figure 6. Circuit diagram of a TEG with DC fan resistance and load resistance

$$V_L = V_{NL} \frac{R_L}{R_{INT} + R_L} \quad (1)$$

$$I_L = \frac{V_L}{R_L} \quad (2)$$

$$P_L = V_L \cdot I_L \quad (3)$$

Steady state energy balance equation can be written by considering following assumptions

- I. Intercept factor can be taken as unity as PDC tracks the sun.
- II. The solar intensity doesn't affect the optical properties of solar PDC.
- III. Solar flux received on the surface of the receiver is distributed uniformly.
- IV. All the equations are incorporated for one dimensional heat transfer analysis.

The contact resistance between the faces of modules, aluminium absorber plate and the surface of aluminium heat sink are neglected.

3. Energy balance for complete PDCSTEG system (Thermal Analysis)

3.1. Solar Parabolic Dish Concentrator

It had been provided by Garg the standard mathematical formulas for computation of the parabolic dish collector parameters, such as mouth opening diameter D , depth of dish h , focal distance f , and aperture angle. The concentrated solar radiation heat received by the absorber/receiver surface, the optical efficiency of PDC and the useful energy delivered by the absorber unit of the solar PDC, which works as input to the TEG are determined from the equations given below [12]-[14] and [35], [36]:

$$q_s = I_B \rho (\tau \alpha)_e \gamma C_R \quad (4)$$

$$\eta_o = \rho_c (\tau \alpha)_e \gamma \quad (5)$$

$$Q_u = q_s A_r - U_L A_r (T_1 - T_a) \quad (6)$$

The useful energy gain in the absorber plate in interval of time is:

$$Q_u = (mC)_{plate} (T_f - T_i) \quad (7)$$

The instantaneous thermal efficiency of the PDC is:

$$\eta_{ith} = \frac{Q_u}{A_{PDC} I_B} \quad (8)$$

3.2. Aluminium absorber Plate

Uncoated aluminium absorber/receiver plate's surface area is exposed to the aperture area of PDC, thus absorbs the concentrated heat and this concentrated heat is then supplied to operation of TEG. Concentration ratio is the determining factor for the amount of heat absorbed and it can be defined as [22]:

$$C_R = \frac{A_{PDC}}{A_r} \quad (9)$$

3.3. Working Principle of Thermoelectric Generator

TEG works on the principle of Seebeck effect. When a temp gradient is applied to the junctions of two dissimilar conductor or semiconductor, an electric potential is developed, this is known as TE effect or Seebeck effect [15], [16].

As per the discussed Seebeck effect the hot junction absorbed the heat flux $\alpha I T_h$ and $\alpha I T_c$ is rejected by the cold junction. There are three additional effects known as Joule heating effect

caused by electric current, heat leakage caused by heat conduction between two junctions and the Thomson heat caused by the temperature gradient and electric current[16], [17]. If the effect of the Thomson heat is considered negligible, then to overcome the Peltier effects, the heat conduction and the joule heating, the equations governing the heat input rate and heat rejection can be obtained by considering the energy supply or removal [20] and [35]-[37].

Heat input to TEG:

$$Q_h = \alpha IT_h + K(T_h - T_c) - 0.5I^2R_{INT} \quad (10)$$

Heat removal from TEG:

$$Q_c = \alpha IT_c + K(T_h - T_c) + 0.5I^2R_{INT} \quad (11)$$

The heat removal rate from the module to the cooling medium is found as:

$$Q_c = k_c(T_{mf} - T_c) \quad (12)$$

By the Newtonion law Q_h and Q_c may be expressed as-

$$Q_h = k_h(T_1 - T_h) \quad (13)$$

$$Q_c = k_c(T_2 - T_c) \quad (14)$$

The electrical power produced by the TE module can be obtained from:

$$P_{TE} = Q_h - Q_c = \alpha I(T_h - T_c) - I^2R_n = R_L I^2 \quad (15)$$

Electrical efficiency of TEG is quantified as:

$$\eta_{TEG} = \frac{P_{TE}}{Q_h} \quad (16)$$

The overall electrical efficiency of the PDCSTEG system is[24]-[28]:

$$\eta = \frac{P_{TE}}{I_B A_{PDC}} = \frac{Q_h}{I_B A_{PDC}} \frac{P_{TE}}{Q_h} = \eta_{PDC} \eta_{TEG} \quad (17)$$

Where η_{PDC} is the thermal efficiency of the solar PDC. η_{TEG} is the electrical efficiency of the TEG. Computation of the properties of bismuth telluride alloys TE modules can be done as [25]:

Seebeck coefficient:

$$\alpha = (22224 + 930.6 T - 0.9905T^2)10^{-9}V/K \quad (18)$$

Electrical Resistivity:

$$\rho = (5112 + 163.4T - 0.6279T^2 + 0.4131T^2)10^{-4}\Omega - m \quad (19)$$

Thermal conductivity:

$$k = (62605 - 277.7T + 0.4131T^2)10^{-4} W/mK \quad (20)$$

For a parabolic dish concentrator and flat plate receiver the following values are approximately valid[8],[38]-

For concentration ratio 100 and beam radiation 1000 W/m² the standard values of TE device parameters are as follows[28], [38].

Table 2. Thermoelectric material (Bi₂Te₃) characteristics and TE device factors on Standard test condition

S.N	Parameters	Value
1.	$C_R = A_{PDC}/A_a$	100
2.	I_B	1000W/m ²
3.	η_{TEG}	0.75
4.	T_h	300 K
5.	α_n	-1.95×10 ⁻⁴ V/K
6.	α_p	2.3×10 ⁻⁴ V/K

7.	ρ_n	$1.35 \times 10^{-5} \Omega\text{-m}$
8.	ρ_p	$1.75 \times 10^{-5} \Omega\text{-m}$
9.	k_n	1.4 W/mK
10.	k_p	1.2 W/mK
11.	A_n/L_n	0.01 m
12.	A_p/L_p	0.01 m
13.	k_h	0.2 W/K
14.	k_c	0.1 W/K

Z and k may be expressed as [28]-

$$Z = \left[\frac{(\alpha_p - \alpha_n)}{\sqrt{k_n \rho_n} + \sqrt{k_p \rho_p}} \right]^2 \quad (21)$$

$$k = \frac{k_n A_n}{L_n} + \frac{k_p A_p}{L_p} = \frac{A_n}{L_n} \left(k_n + \sqrt{\frac{k_n k_p \rho_p}{\rho_n}} \right) \quad (22)$$

For the geometric configuration of the TEG the optimal conditions may expressed as [9],[10]-

$$\frac{L_n/A_n}{L_p/A_p} = \sqrt{\frac{k_n \rho_p}{k_p \rho_n}} \quad (23)$$

where A_p and L_p are the cross-sectional area and the length of the p -type semiconductor element.

The ratio of area to length of the TE element can be defined as aspect ratio.

Thermoelectric maximum efficiency and Figure of merit [25],[27]:

$$\eta_{TEG} = \frac{T_h - T_c}{T_h} \frac{\sqrt{(1+ZT)} - 1}{\sqrt{(1+ZT)} + \frac{T_c}{T_h}} \quad (24)$$

$$ZT = \frac{\alpha^2 \sigma T}{k} \quad (25)$$

Where $\alpha = \frac{\Delta V}{\Delta T}$ is the Seebeck coefficient, σ is the electrical conductivity, k is the thermal conductivity which can be divided into two parts (k_e and k_l the electrical and lattice respectively)[7]and T is the average temperature $T = \frac{T_h + T_c}{2}$, Z is the effective figure of merit across the temperature gradient, $\frac{T_h - T_c}{T_h}$ is Carnot efficiency[8].

4. Results and Discussion

The performance characteristics of a class of thermoelectric generator using solar energy as a heat source are discussed through a thermodynamic model. There are always four irreversibility exist in a solar thermoelectric generator like-finite-rate heat transfer between the thermoelectric device and the external heat reservoirs, heat leakage through the thermoelectric device, ohmic heat generated inside the thermoelectric device and heat loss in the solar absorber[19], [28]. On the performance parameters these are investigated with the help of non-equilibrium thermodynamics and finite-time thermodynamics. The variation of Solar Radiation (Global, Concentrated, Diffuse, Beam) with respect to time from 800 hrs to 1645 hrsthroughout the day at each time interval of 15 minute with total 36 observations were recorded. All the radiation between minimum and maximum value during 1100 hrs to 1400 hrs varies as Global Radiation I_G (810-1020 W/m²), concentrated radiation I_C (1200-1621 W/m²), diffuse radiation I_D (99-151

W/m^2), beam radiation I_B (659-892 W/m^2) as shown in **Figure 7**. Parameters T_a , T_h , T_c , V_a , Rh_a , V , I are also observed at every 15 minutes interval from 800 hrs to 1645 hrs and I_B , T , ΔT , P are calculated and the overall efficiency of PDCSTEG, the optimal operating temperature of solar receiver/absorber, the optimal matched load resistance and some other novel results are found.

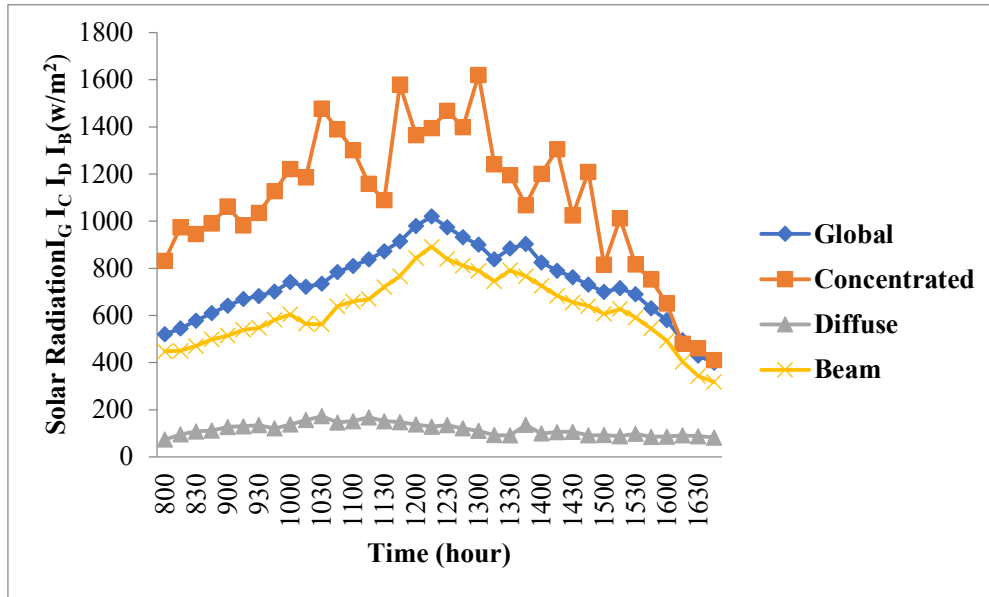


Figure 7. Variation of solar radiations during sun shine hour at $23^{\circ} 16'N$, $77^{\circ} 36'E$

PDCSTEG is simply constructed consist of a TEG and solar collector/concentrator as shown in **Fig. 3**. The p -type and n -type legs are the primary elements of TEG [26].

The amount of energy $I_B A_{PDC}$ is received by the aperture area A_{PDC} (1.54 m^2) by the concentrator and it supplied heat to the receiver/absorber with aperture area A_r at the rate q_s , thus the total insolation $q_s = I_B \rho_c (\tau \alpha)_e \gamma C_R$ is received by the absorber is expressed by **Equation (4)**[19], where I_B is the solar insolation.

The reflectivity of parabolic dish material (Anodized aluminium) is 0.84, effective transmissivity and absorptivity product of the receiver surface is 0.80. The PDC concentrate only the beam radiations that start to raise the temperature of hot side. The heat input rate to the thermoelectric generator from the solar receiver/absorber is Q_h at temperature T_h and heat rejection from TE device to heat sink takes place at rate Q_c at temperature T_c according to **Equation (10 and 11)**[29]. The heat leakage through the TE device is Q_k and heat loss of the solar receiver/absorber is considered as $Q_L = U_L A_r (T_1 - T_a)$ according to **Equation-(6)**[30].

The electrical power P , at current I is produced by the TEG and it is transferred to the load resistance R_L and fan resistance R_{FAN} as per the Equations (1, 2, 3). T_h and T_c are the temperatures of the two junctions in the thermoelectric device, whose variation during 1100 to 1400 hrs was observed as hot side temperature (150-210 $^{\circ}C$), cold side temperature (37-45 $^{\circ}C$) and hence the average temperature T (93.5-127.5 $^{\circ}C$), ΔT (113-165 $^{\circ}C$) at ambient temperature (38.9-40.2 $^{\circ}C$) are shown in **Figure 8**. The useful energy delivered to thermoelectric generator

by the receiver unit is computed by $Q_u = q_s A_r - U_L A_r (T_r - T_a)$ as per **Equation (6)**, where A_r is the absorber area of the solar collector and $\eta_{\text{ith}} = \frac{Q_u}{A_{PDCI} I_B}$ is the instantaneous thermal efficiency as per equation (8)[16].

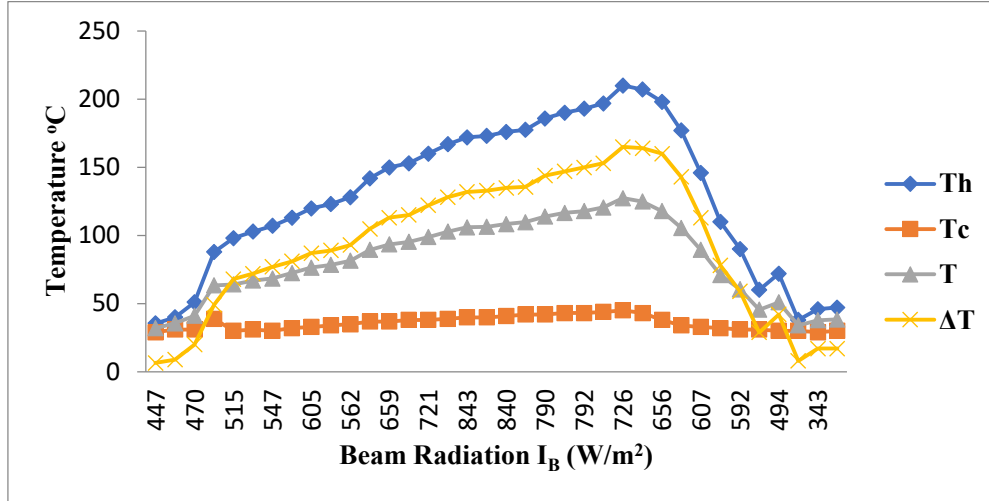


Figure 8. Variation of temperatures with beam radiations

Here, Seebeck effect is the most important factor due to which TE device works as a generator, heat flux $\alpha I T_h$ is absorbed at hot junction and $\alpha I T_c$ is the heat flux rejected at cold junction, where α is the Seebeck coefficient. α does not only depend upon the properties of semiconductor material but also is a function of temperature according to the **Equation (18)**[32] i.e., $\alpha = \alpha(T)$. Three additional effects also exist in TE device: Joule heating due to the electrical current, heat leak between the two junctions, Thomson heat due to both the temperature gradient in the TE device and the electrical current[33]. The TE device which has negligible Thomson coefficient, their performance is not influenced by the Thomson coefficient and α may be approximately considered as a constant[39]. Thomson heat is taken as negligible in this research. The TE device is insulated both electrically and thermally from the surrounding except at the junction-reservoir contacts, it is assumed for the purpose of analysis, such that the net rates of heat input q_h is $\alpha I T_h + K(T_h - T_c) - 0.5 I^2 R_{INT}$ and heat rejection q_c is $\alpha I T_c + K(T_h - T_c) + 0.5 I^2 R_{INT}$ as per **Equations (10, 11)**. Where K and R_{INT} are the thermal conductance and the total internal electrical resistance of the TE device. Joule heat produced inside the thermoelectric device flows equally to the hot and the cold junctions that is why a factor of 1/2 in $R_{INT} I^2$ term appears[40]. According to the above assumptions α may be considered as a constant, the electrical power P produced by TE modules is $q_h - q_c$ which is equal to $\alpha(T_h - T_c)I - R_{INT} I^2 = R_T I^2$ as per **Equation (15)**[41]. If α is considered as function of temperature and the effect of the Thomson heat has to be considered[42], the performance of PDCSTEG remains to be investigated further. The more analytical model for a PDCSTEG can be established by considering the effect of the irreversibility of finite-rate heat transfer between the TE device and its external heat reservoirs. Newtonian law is also obeyed by the heat transfer so q_h and q_c may be expressed as from **Equations (13, 14)**-
 $Q_h = k_h(T_1 - T_h)$ and $Q_c = k_c(T_2 - T_c)$

Where k_h is the thermal conductance between the solar absorber and hot junction and k_c is the thermal conductance between the cold junction and the heat sink. Using the above equations, we derived the efficiency of a PDCSTEG and discuss its optimal performance.

4.1. Optimization of Load for a PDCSTEG system in view of no load and loaded tests-

In this project we used TEG module (32 × 32 mm) for our experiment. Bismuth telluride alloy is the material of which module is made of and the length of the TE element is 1.72 mm. Specifications of TEG according to the supplier are-figure of Merit of TE material ($Z=1$), rated power 5 W, rated voltage 12 V, rated current 1 A at $T_h = 220$ °C and $T_c = 30$ °C. The internal resistance of TEG module is 1.84 Ω at maximum working temperature of 220 °C. The maximum processing temperature of TEG is 220 °C. Open circuit test and load tests ($R_{fan}=96$ Ω, $R_L=16.94$ Ω, $R_T=R_{fan}||R_L=14.4$ Ω) are performed to analyse the performance of TE module, but the TEG produces output voltage in the range (6.3-10 V), current in the range (0.437-0.7 A) and Power in the range (2.94-6.94 ≈ 7 W). The PDC concentrate only the beam radiations that start to raise the temperature of hot side. The Voltage build up process starts at T_h 35.5 °C with a value of 0.75 V and reaches to the value of 10 V at 210 °C instead of rated voltage of 12 V, current 0.7 A instead of 1 A and power 6.94 ≈ 7 W instead of 10 W for the solar beam radiation ranging from 726 w/m², because of the decrement in ΔT due to increased air velocity and relative humidity, these all parameters doesn't match with the supplier's specification. The maximum overall efficiency of PDCSTEG system for hot Side Temperature (T_h) 210 °C, Cold Side Temperature (T_c) 45 °C, Average receiver temperature (T) 127.5 °C, maximum output Voltage 10 V, Current 0.7 A, Power 7 W is obtained 0.6207%.

Maximum power to the load is transferred in the case only when load resistance equals the internal resistance of the TEG. Ironically, at this operating point, equal amount of power will be dissipated within both the load and the internal resistance of the generator (i.e., electrical efficiency will be 50%) [34]. To obtain maximum electrical power output the load resistance is kept equal to internal resistance of TEG. The overall efficiency of the PDCSTEG system can be better for the higher value of beam radiations (more sunshine) with less wind velocity and relative humidity [35]. Further discussion about the results and optimization of load is as follows.

The device was kept under sunshine for an hour so that it could achieve steady state. As the incoming solar radiation increases during the day, the hot side temperature increases, the DC fan maintains cold side temperature between 35-42 °C during 1100 hrs to 1400 hrs. At the starting of the day around 800 hrs when $T_h = 35$ °C and $T_c = 27$ °C, No load voltage or open circuit voltage build up process starts up at ΔT 8 °C and observed as 0.78 V as shown in **Figure 9**. As the time passes after 800 hrs solar radiation increases, which leads to increase hot side temperature that raises open circuit voltage. The maximum no load voltage is achieved as 11.27 V at 1400 hrs when beam radiations are observed as 726 W/m².

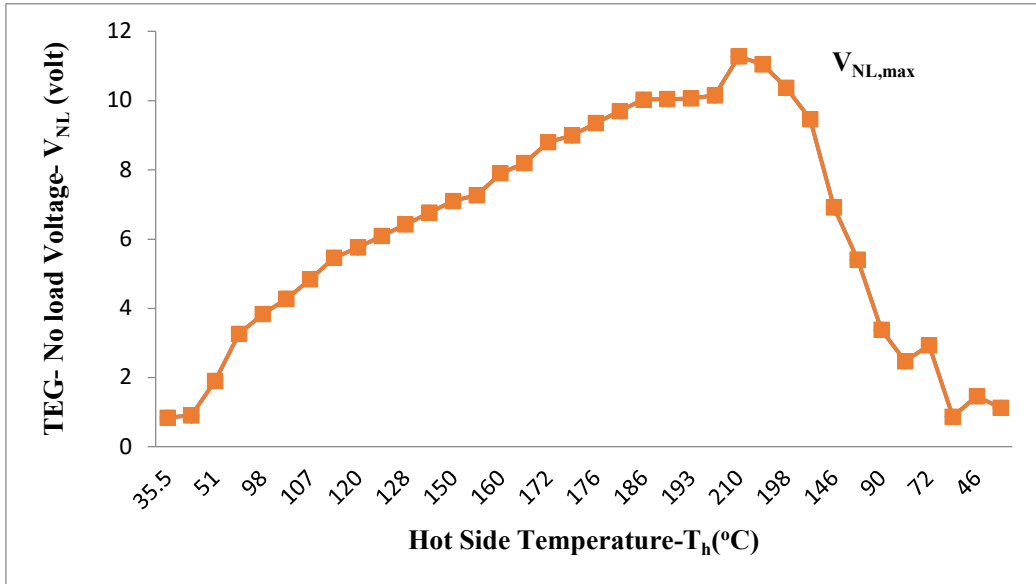


Figure9. Open Circuit Voltage v/s Hot side Temperature

The no load test and load test were conducted simultaneously on the TEG after each 15 minute interval. For every beam radiation value open circuit voltage was observed, at the same moment TEG was loaded with connected half load and full load (R_T) consecutively and hence all other parameters like voltage, current and power of TEG were observed and calculated as shown in Fig. 10. The maximum load voltage 10V, load current of 0.694 A were observed and power 7 W calculated for no load voltage (TEG output voltage) 11.27 V at solar beam radiation of 726 W/m².

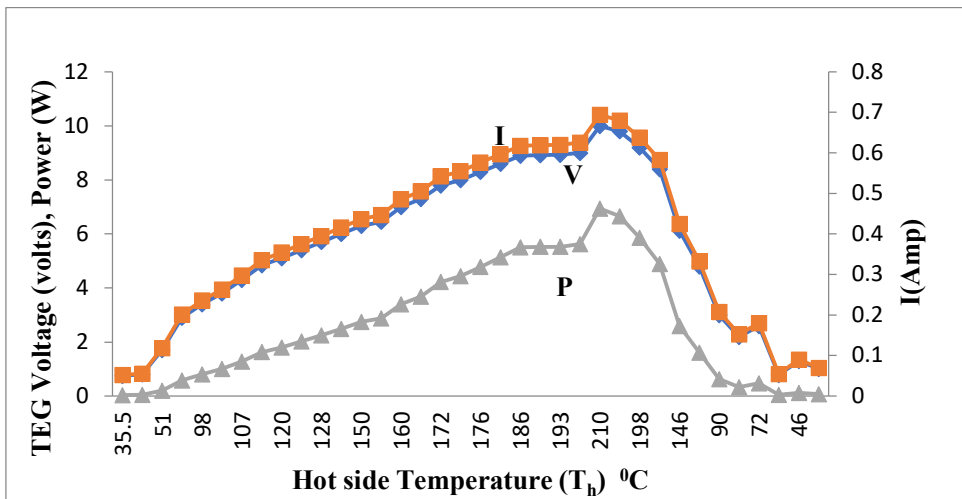


Figure10. Variation of output TEG voltage, Current and power for various operating hot side temperature (T_h v/s V_L , I, P curve, T_c : 35-43 °C, R_{fan} =96 Ω R_L =16.94 Ω R_T =14.4 Ω)

The electrical power output of a thermoelectric generator is $P_{TE} = I_B A_{PDC} \eta$ as per Equation (15). It can be easily proved that when the efficiency of a PDCSTEG with a given quantity $I_B A_{PDC}$ attains its maximum, the power output also attains maximum. It is here clearly manifested that both the maximum power output and the maximum efficiency of a PDCSTEG

are identical states. But maximum power transfer to the load R_L is so important in designing TEG systems. TEGs inherently don't work as regulated power supplies[43]. At any given ΔT , if the load resistance decreases, the output voltage also decreases and as the load resistance increases, the output voltage will also increase[44]. There is no inherent output regulation (We can provide additional circuit to regulate the voltage). Because every TEG has considerable amount of internal resistance, it refers that as more current will be drawn by the electrical load (e.g., as load resistance decreases), more of the available power will be dissipated within the TEG. Moreover there will be a considerable voltage drop across this internal resistance. Analysis of the voltage drop with the help of electrical model of TEG system is accomplished in this article. If there is a no-load voltage (i.e., the open-circuit voltage output of a TEG) applied to a series circuit consisting of the module's internal resistance R_{INT} and the total electrical load R_T as shown in **Figure6**, there will be a voltage drop in proportion to the resistance according to voltage divider rule. Thus, if we consider no-load voltage 7V, the internal resistance is 1.86Ω and the Full load $R_T = 14.4 \Omega$ ($R_T = R_{fan} \parallel R_L$), then from equation-(1) there would be a 6.2 V drop across the load. This decrement in load voltage can be seen in **Figure11**.

$$V_L = V_{NL} \frac{R_T}{R_{INT} + R_T} = 7V \frac{14.4\Omega}{1.86\Omega + 14.4\Omega} = 6.2V$$

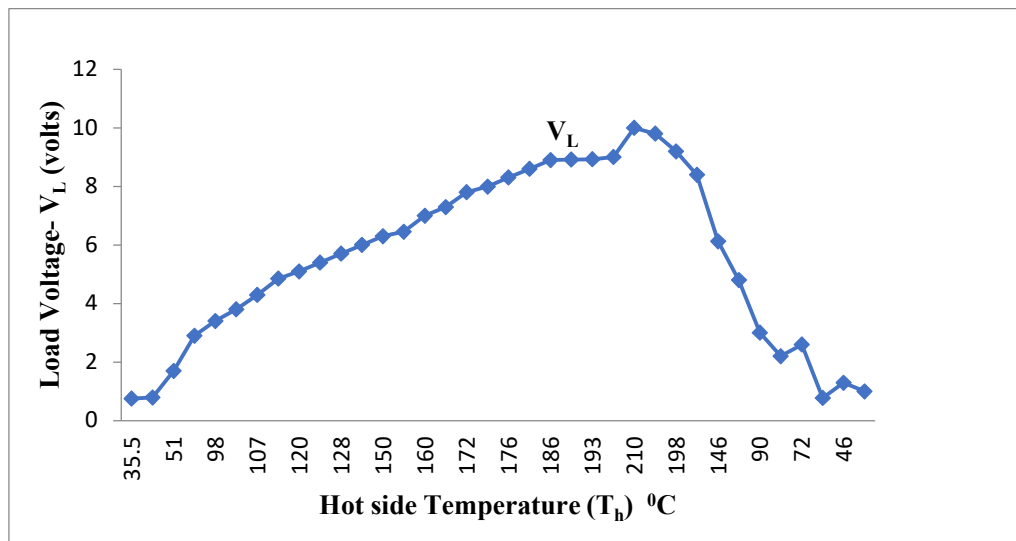


Figure11. Variation of Load Voltage with Hot side Temperature (T_h v/s V_L curve, T_c : 35-43 °C, $R_{fan}=96 \Omega$ $R_L=16.94 \Omega$ $R_T=R_{fan} \parallel R_L=14.4 \Omega$)

Therefore, the maximum power transfer to the load is a major concern here. Therefore for any electrical circuit maximum power can be transferred to the load if the load resistance equals the internal resistance of the voltage source (TEG)[43], [44]. Here it is to be noted that this point of operation will not provide us the maximum amount of voltage or current, but the greatest power can be derived at that point. For any no load voltage the following formulas are

used to determine load voltage, current and power for various load resistances from **Equations (1, 2, 3)**:

$$V_L = V_{NL} \frac{R_L}{R_{INT} + R_L}, I_L = \frac{V_L}{R_L}, P_L = V_L \cdot I_L$$

The variation of TEG output current and power delivered to load with load voltage can be seen in **Figure 12**. with rise in TEG generated voltage, the load voltage also increases, the demand of load power at required load current is fulfilled. The maximum power is delivered to the load at maximum voltage.

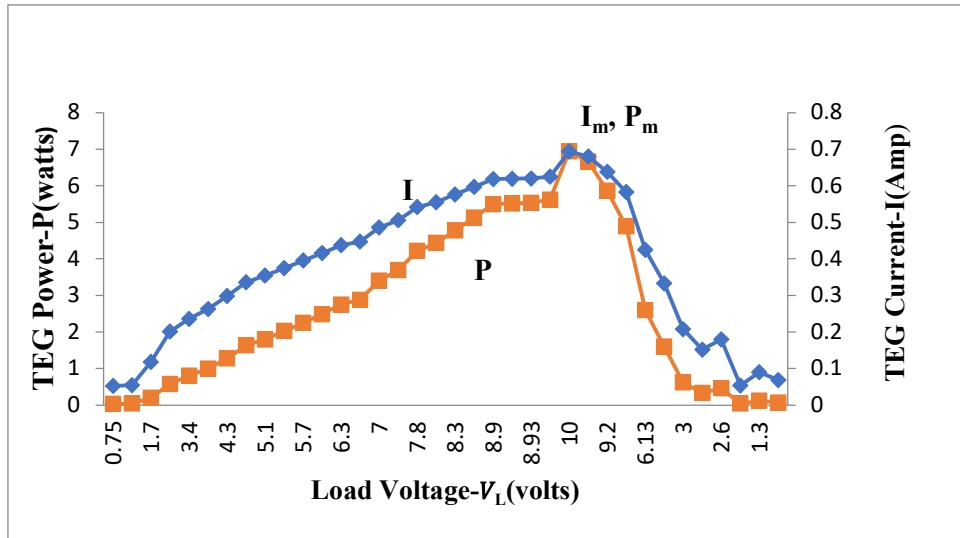


Figure 12.Electrical performance of thermoelectric module (I-V and P-V curve, T_c : 35-43 $^{\circ}$ C, R_{fan} =96 Ω R_L =16.94 Ω R_T =14.4 Ω)

It is fairly tricky to match the loads. It can be easily done when a TEG is customised for a particular project, then the optimization of the pallet configuration can be done for the specific application [20], [30]. On the other hand, the best job of load-matching is the series/parallel module combination, for which the designer is left to arrive at. Moreover complicating matters in many cases will be the fact that operating conditions may change over time and our design may be matched for one set of circumstances but not for another[25],[26]. For the dynamic ambient environment and/or variable load resistance, the TEG must be designed to the worst case and then manage surplus capacity with a regulatory circuit[26], [27].

Sometimes maximum power transfer couldn't be the priority, especially in those systems whose heat source is not waste heat. Here power conversion efficiency(which occurs at a somewhat different operating point) may be the greater issue. Even then TEG is made to compromise a bit toward enhancing power transfer[27], [19]. A significant power boost can be achieved by sacrificing a little bit of efficiency. Practically most TEG system designs will be at least somewhat mismatched[29], [30]. For a discrete building block (i.e., individual TEG modules) only a given resistance with series/parallel combination can be approximated. Generally, it is better to err on the side of having load resistance exceed internal resistance (efficiency is a much more slippery slope when it is the other way around). In the general cases, we obtain the required load resistance at the maximum power output, i.e. the optimal load

matching. In the special case the optimal value of the load resistance must be [37]-

$$R_{L,opt} > R_{INT}$$

The calculative results of the optimal load resistance provide an important theoretical basis for the optimal operation of PDCSTEG.

4.2. Variation of internal resistance with operating temperature and dynamic ambient conditions-

Design solutions of TEGs are significantly depend on temperature-dependent properties of TE material according to **equation (18, 19 and 20)**, Which create more challenges in arriving at design solutions. The module has internal resistance of 1.84Ω at an average temperature ($T = \frac{T_h+T_c}{2}$) of 115°C , it may reach 2.84Ω at 150°C . This affect output voltage, current and power as operating temperature changes. For this module for instance, if 115°C is the average operating temperature, the no-load voltage is 10 V and the load resistance is 14.4Ω , it gives a resulting load voltage of 8.86V with a load current of 0.52 amps ($P_L = 4.6\text{ W}$). Due to some dynamic ambient conditions throughout the day and continuous operation if the average operating temperature then drifted to 150°C while keeping constant no-load voltage, there will be the decrement in load voltage to 8.3 V with a load current draw of 0.50 A ($P_L = 4.17\text{ watts}$ -nearly a 9.3% decrease). Therefore, if there is any variation in operating conditions, there will be a need to look at the range of module resistance that may provide result according to variable ambient condition. So it is quite clear that TEG system designing should be done, keeping in mind worst case condition and ensure that the system should provide sufficient power even when ΔT is low and high current demand and it should have the capacity of excess generation at all other operating points.

4.3. Maximum efficiency of PDCSTEG system-

As per equation (17, 24 and 25)

$$\eta = \frac{P_{TE}}{I_b A_{PDC}} = \frac{Q_h}{I_b A_{PDC}} \frac{P_{TE}}{Q_h} = \eta_{PDC} \eta_{TEG}$$

shows clearly that the efficiency η of a PDCSTEG is equal to the product of the thermal efficiency η_{PDC} of the solar collector and the TEG efficiency η_{TEG} of the thermoelectric generator. For a PDC as a heat engine [38] η_{PDC} decreases with an increase in the operating temperature T_h of the solar collector after an optimum temperature $T_{h,opt}$ and η_{TEG} increases with an increase in the operating temperature T_h upto 210°C . It clearly specifies that there should be an optimum operating temperature $T_{h,opt}$ at which the efficiency of the PDCSTEG will be maximum[5], [38]. By incorporating above information, we plotted the curve of PDCSTEG efficiency varying with the operating temperature of the solar absorber/receiver, as shown in **Figure13**. It is seen from **Figure13** that for a given area A_r , the efficiency increases when hot side temperature increases upto 210°C . There will be an optimal maximum current I_m at which the efficiency of PDCSTEG will be maximum, as shown in **Figure 12 and Figure 13**.

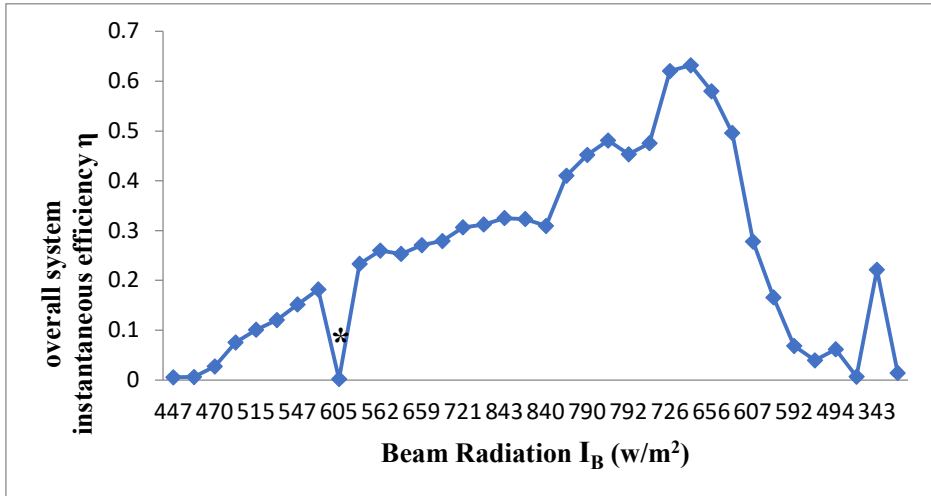


Figure13. Variation of Instantaneous overall PDCSTEG system efficiency with beam radiation η_{max} is an important parameter of PDCSTEG, because it determines an upper bound for the efficiency of a class of TEG, whose source is solar energy. It is worthwhile to note that the electrical current at the maximum efficiency η_{max} is another important parameter of PDCSTEG.

Instantaneous maximum overall system efficiency of PDCSTEG from Equation-17:-

$$\eta_{max} = \frac{\text{Maximum Power Output}}{\text{Power input}}$$

Maximum Power Output = 6.94 \approx 7 w

Aperture Area of the PDC = 1.54m²

Beam radiation = 726 w/m²

$$\text{Power i/p} = \text{Aperture Area of the PDC (m}^2\text{)} \times \text{Beam radiation(W/m}^2\text{)}$$

$$\eta_{max} = 0.6207 \%$$

It can be observed clearly from **Figure 12 and Figure 13** that for a given receiver area A_r , both η_{max} and I_m increases when ΔT increases and both decrease when ΔT decreases. At * point the efficiency is very low 0.0019%, because ΔT is very low due to dynamic ambient conditions. There is always a finite-rate heat-transfer between the TE device and the external heat reservoirs and heat leakage between two junctions of TE device so the maximum efficiency is achieved at the maximum electrical current I_m . **Figure 13** shows the instantaneous overall system efficiency of the PDCSTEG ranges as (0.2709-0.6207%), which is to be as low as 0.2709% at lower beam radiation of 659 W/m² at operating temperature of 150 °C. Increment in operating temperature gradually increases the overall system efficiency. The PDCSTEG achieve a maximum efficiency of 0.6207% when the solar beam radiation reaches the value of 726 W/m² at temperature 210°C. Increase in velocity of ambient air and relative humidity decrease the operating temperature of hot side and cold side that results decrease in ΔT , which ultimately reduces the overall system efficiency and vice-versa. Air velocity during the whole day varies in the range of (0.18-1.20 m/s) and relative humidity is in the range of (14.2-21.2%).

5. Artificial Intelligence in PDCSTEG

ANN commonly referred to as neural networks, had been extensively used in a large variety of programs. Those applications consist of pattern popularity, function Approximation, optimization, simulation, and estimation can be automated amongst many different software

regions and furthermore studies have produced a large number of community Paradigms. Nowadays, ANN have been skilled to remedy Complex troubles which are hard to resolve by way of conventional Techniques. ANN conquers the restrictions of the Traditional methods by means of extracting the desired statistics viause of the input statistics. An ANN does now not need such a selected Equation shape, however it requires enough input-output records. Additionally, it may continuously be re-educated, so that it may readily adapt to new facts. An ANN has been investigated to cope with the troubles related to incomplete or obscure input facts. An essential degree of a neural network is the training Step, in which an input is added to the network collectively with the favoured output; the weighs and bias values are initially Chosen randomly and the weighs are adjusted so that the Network tries to produce the desired output. The weighs after training, contain significant statistics, while before training, they're random and don't have any means. When a Great level of overall performance is reached, the training stops, and the network makes use of the weighs to make choice. Many Alternate education techniques are being incorporated including back propagation that has different editions. The purpose of any training set of rules to limit the mistakes including mean % Error, root-mean-square (rms) etc. An ANN model records processing paradigm that is inspired by way of the way the biological apprehensive structures such as the brain manner information. The key element of this paradigm is the radical structure of the statistics processing machine. It Composed of a big range of distinctly inter related Processing factors (neurons) running in unison to clear up Particular trouble. The network usually consists of an input Layer, one hidden layer and an output layer. Ann is like a human being that Examine through instance as biological structures involves Adjustment to the synaptic connections that exist among the Neurons. ANNs operate a complete lot like a “black field” version, requiring no specific statistics about the function. An artificial neuron is a tool with many inputs and one output. The neuron has modes of operation; the Education mode and the checking out mode. In the training mode, Neuron can be trained to fireplace (or not now state) for precise input Styles. In the checking out mode, whilst a taught input sample is detected on the entry level, its associated output will become the modern-day Output.

5.1. Heat maps of PDCSTEG

Each square shows the correlation between the variables on each axis. Correlation ranges from -1 to +1. Values closer to zero means there is no linear trend between the two variables. While values closer to 1 the correlation more positively correlated; that is as one variable increases, so does the other and as it reaches to closer to 1 the stronger the relationship is. A correlation closer to -1 is similar, however instead of both increasing, one variable will decrease as the other increases. The diagonals are all 1/dark green because those squares are correlating each variable to itself (so it's a perfect correlation). For the rest of the values, the larger the number and darker the colormanifest the higher correlation between the two variables. The plot as shown in **Figure14**is also symmetrical about the diagonal since the same two variables are being paired together in those squares.

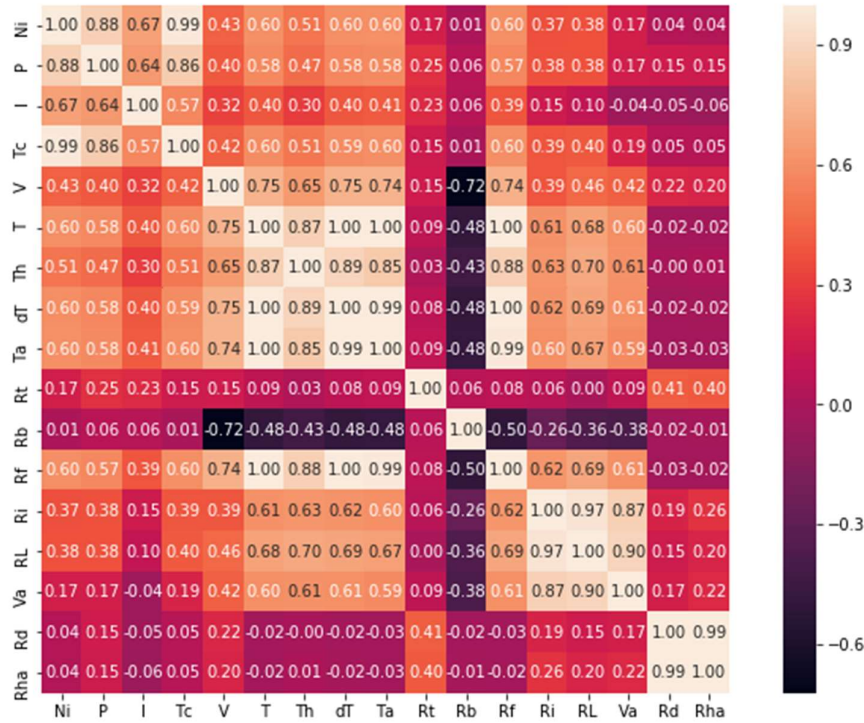


Figure 14. Visual representation of Heat map

The PDCSTEG system modeled by ANN has eight inputs and one output. The input variables of Solar collector systems are the (Rb) beam radiation, hot side temperature (Th), (Tc) cold side temperature, (dt) temperature difference between hot and cold side, (Rha) relative humidity, (V) voltage, (I) current, (RL) load resistance, and (Rt) total resistance all these parameters were taken into consideration to calculate and predict (Ni) total efficiency of the system. All network calculations were performed using python Jupyter lab Platform. The original data set was having 19 features which was reduced to 9 data features on the basis of heatmap used for correlation between different factors. The data set for the efficiency of the system available included 108 data pattern for each. From these 81 data patterns were used for training the ANN. The remaining 27 patterns were used as the test data set. The Architecture for ANN is shown in **Figure15**, the optimizer used was Adam optimizer or adaptive moment estimation which is an algorithm for optimization technique for gradient descent.

5.2. The ANN Model of PDCSTEG (with 8 inputs)

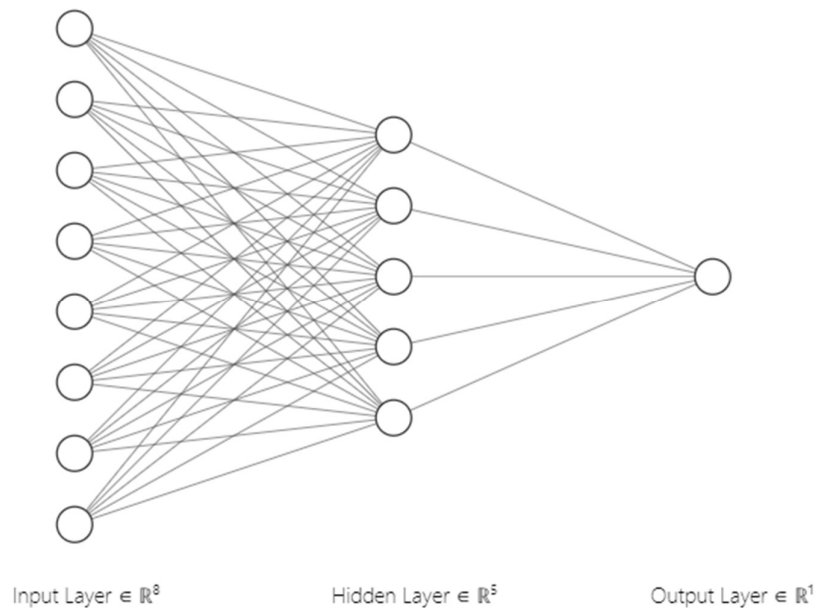


Figure15. Diagrammatic representation of Multilayer Neural network model

The predicted values obtained from the ANN model for PDCSTEG is shown in **Figure16** reveal the best trained data with minimum error. Efficiency with a mean square error (MSE), root mean square error (RMSE), mean absolute error value is 0.00223354, 0.04726043 and 0.02570740 respectively. In this case, these results confirm that the experimental values are closer to ANN predicted results.

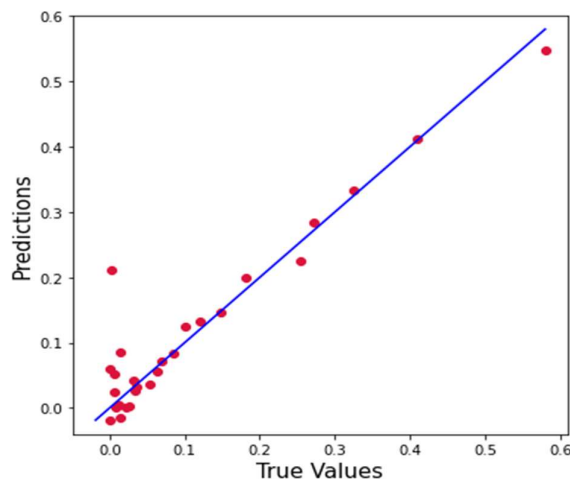


Figure16. Prediction Curve for efficiency (Best Linear Fit For predicted And True values)

6. Conclusions and future phase of work

An experimental prototype of Solar concentrating thermoelectric generator using parabolic dish concentrator, absorber/receiver, heat sink cooling system and TEG modules is fabricated

and the potential of thermo electric cells combined with concentrating solar energy as a power generation system has been tested and illustrated. The following conclusions were drawn:

- I. By incorporating parabolic dish concentrator technology without maximum power point tracking overall PDCSTEG system maximum efficiency is achieved as 0.6207% at the solar beam radiation of 726 W/m^2 and a minimum of 0.2709% at a minimum solar beam radiation of 659 W/m^2 during 1100 hrs and 1400 hrs for the 10 W capacity TEGs with passive air cooling and without any maximum power point tracker.
- II. The parameters are achieved as hot side temperature 210°C and Cold side temperature 45°C that's why $\Delta T=165^\circ\text{C}$ instead of 170°C is achieved i.e ΔT decreased by 5°C and hence maximum Power output approximately $6.94 \text{ W} \approx 7 \text{ W}$ at 10 V voltage and 0.694 A current with an overall system efficiency of 0.6207% with passive air cooling and without any maximum power point tracker.
- III. The power transfer to the load can be maximum, only when the load resistance would be equal to internal resistance of the TEG module.
- IV. The maximum power output 7W is found just near to rated power of 10W as specified by supplier, however not matched with the supplier's specifications. This Power gap is mainly caused by the reduction in ΔT due to dynamic ambient conditions, like increased air velocity and humidity.
- V. The experimental and theoretical values of generated power of the PDCSTEG were within 30% accuracy.
- VI. The experimental results showed a considerable agreement with the mathematical model as well as its potential applications without considering losses.
- VII. Further investigation of the PDCSTEG can be studied by incorporating all the losses. It is observed that the perspective applications for such power system is strongly depend on the development of the thermoelectric material, types of concentrator, various absorber, absorber coating, various substrates, various heat sinks, therefore research about exploring the latest improved TE material with other design parameters under the current PDCSTEG system is recommended. Performance can be improved by implementing maximum power point solar tracker however it increases the cost of TEG power generation.
- VIII. PDCSTEG could be a perspective and feasible device of the renewable energy based power source from small scale to large scale application without harming environment.

Authors Contribution:

Sanjeev Kumar Bhukesh: Conceptualization, Methodology, Writing- Original draft preparation, Investigation, Data curation, **Anil Kumar:** Supervision, Reviewing and Editing, **Suresh Kumar Gawre:** Supervision, Reviewing and Editing

Acknowledgement: Authors are highly thankful to Maulana Azad National institute of Technology, Bhopal, India for providing all basic research facility.

Data Availability Statement:

The data that support the findings of this study are available from the corresponding author upon reasonable request.

Declaration of competing interest:

The authors declare that they have no known competing financial interests or personal relationships that could have appeared to influence the work reported in this paper.

Nomenclature

- A_{PDC} : Aperture area of the solar parabolic dish collector, m^2
 A_r : Aperture area of the receiver plate, m^2
 A_n : Cross-sectional area of n-type TE element leg
 A_p : Cross-sectional area of p-type TE element leg
 C : Coefficient of performance
 C_R : Concentration ratio
 I_G : Global radiation W/m^2
 I_C : Concentrated Radiation W/m^2
 I_D : Diffuse Radiation W/m^2
 I_B : Beam Radiation incident on the concentrator surface, W/m^2
 I : Output Electric Current **A (Ampere)**
 I_L : Load current **A (Ampere)**
 I_m : Maximum output Electric Current **A (Ampere)**
 K : Thermal conductance of the thermoelectric device, **W/K**
 k : Thermal conductivity of thermoelectric material, **W/m-K**
 K_c : Heat transfer coefficient between the module cold side and the cooling medium, **W/m²K**
 k_h : Thermal conductance between the solar receiver/absorber and hot junction, **W/K**
 k_c : Thermal conductance between the cold junction and the heat sink, **W/K**
 L_n : Length of n-type TE element leg
 L_p : Length of p-type TE element leg
 m : mass of the receiver plate, **Kg**
 P_{TE} : Electrical power produced by TE module, **W**
 P_L : Power delivered to load
 q_s : Heat supplied to the absorber/receiver, **W/m²**
 Q_h : Absorbed heat flux at hot junction, **W**
 Q_C : Heat rejection from the TEG/Heat flux rejected at cold junction, **W**
 Q_u : Useful energy delivered to TEG by the absorber, **W**
 Rh_a : Relative Humidity **%**
 R_{INT} : Internal resistance of TEG, **Ohm**
 R_{fan} : DC fan resistance **Ohm**
 R_L : Load resistance **Ohm**
 $R_{L,opt}$: Optimum load resistance, **Ohm**
 R_T : Total electrical load resistance **Ohm**
 T_a : Ambient Temperature **°C**
 T_1 : Receiver/absorber plate temperature **°C**
 T_2 : Heat sink temperature **°C**

T_h : Hot junction side Temperature of the TEG $^{\circ}\text{C}$
 $T_{h,opt}$: Optimum hot side temperature of the TEG $^{\circ}\text{C}$
 T_c : Cold junction side Temperature of the TEG $^{\circ}\text{C}$
 T : Average Temperature of receiver/absorber $^{\circ}\text{C}$
 ΔT : Temperature difference between hot side and cold side $^{\circ}\text{C}$
 T_{mf} : Mean fluid (air) temperature at aluminium sink box device $^{\circ}\text{C}$
 T_f : Final temperature of the receiver/absorber plate $^{\circ}\text{C}$
 T_i : Initial temperature of the receiver/absorber plate $^{\circ}\text{C}$
Time: Hours
 V_a : Air Velocity m/s
 V_L : Load voltage V
 V_{NL} : No load voltage V
 U_L : Overall heat Loss Coefficient (radiative, conductive, convective)
 V : Output voltage V (**Volt**)
 ΔV : Change in voltage with change in temperature
 Z : Figure of merit of thermoelectric material

Abbreviation

Min: minimum
Max: maximum
PDCSTEG: Parabolic Dish concentrated Solar Thermoelectric Generator
PDC: Parabolic dish concentrator
STC: Solar Thermal collectors
TEG: Thermoelectric Generator
TE: Thermoelectric
hrs: hours

Greek Symbols

η_o : Instantaneous optical efficiency of PDC %
 η_{ith} : Instantaneous thermal efficiency of PDC %
 η_{TEG} : Instantaneous electrical efficiency of TEG %
 $\eta_{TEG max}$: Instantaneous maximum electrical efficiency of TEG %
 η : Instantaneous overall system efficiency %
 η_{max} : Instantaneous maximum overall PDCSTEG system efficiency %
 γ : Intercept factor
 τ : transmissivity of the receiver
 α : absorptivity of the receiver
 $(\tau \alpha)_e$: Effective transmissivity and absorptivity product of receiver surface
 ρ_c : Reflectivity of the concentrating surface
 ρ : Electrical resistivity of the thermoelectric material
 α : Seebeck coefficient of thermoelectric material

References

- [1] R. Prävǎlie, C. Patriche, and G. Bandoc, "Spatial assessment of solar energy potential at global scale. A geographical approach," *J. Clean. Prod.*, vol. 209, pp. 692–721, 2019,

- doi: 10.1016/j.jclepro.2018.10.239.
- [2] M. K. Hairat and S. Ghosh, "100 GW solar power in India by 2022 – A critical review," *Renew. Sustain. Energy Rev.*, vol. 73, no. November 2016, pp. 1041–1050, 2017, doi: 10.1016/j.rser.2017.02.012.
- [3] R. Singh, "Energy sufficiency aspirations of India and the role of renewable resources: Scenarios for future," *Renew. Sustain. Energy Rev.*, vol. 81, no. June, pp. 2783–2795, 2018, doi: 10.1016/j.rser.2017.06.083.
- [4] E. Ogbonnaya and L. Weiss, "Micro Solar Thermal Power Harvesting using Thermoelectric Generator," *Natl. Soc. Black Eng. Proc. 38th Annual Conv. Pittsburgh, PA*, pp. 88–95, 2012, [Online]. Available: http://www2.latech.edu/~lweiss/Site/Vitae_files/NSBE_2012.pdf.
- [5] D. Kraemer *et al.*, "Concentrating solar thermoelectric generators with a peak efficiency of 7.4%," *Nat. Energy*, vol. 1, no. 11, 2016, doi: 10.1038/nenergy.2016.153.
- [6] W. He, G. Zhang, X. Zhang, J. Ji, G. Li, and X. Zhao, "Recent development and application of thermoelectric generator and cooler," *Appl. Energy*, vol. 143, pp. 1–25, 2015, doi: 10.1016/j.apenergy.2014.12.075.
- [7] D. K. Aswal, R. Basu, and A. Singh, "Key issues in development of thermoelectric power generators: High figure-of-merit materials and their highly conducting interfaces with metallic interconnects," *Energy Convers. Manag.*, vol. 114, pp. 50–67, 2016, doi: 10.1016/j.enconman.2016.01.065.
- [8] M. L. Olsen *et al.*, "A high-temperature, high-efficiency solar thermoelectric generator prototype," *Energy Procedia*, vol. 49, pp. 1460–1469, 2013, doi: 10.1016/j.egypro.2014.03.155.
- [9] M. Hamid Elsheikh *et al.*, "A review on thermoelectric renewable energy: Principle parameters that affect their performance," *Renew. Sustain. Energy Rev.*, vol. 30, pp. 337–355, 2014, doi: 10.1016/j.rser.2013.10.027.
- [10] G. Zhang *et al.*, "A comprehensive design method for segmented thermoelectric generator," *Energy Convers. Manag.*, vol. 106, pp. 510–519, 2015, doi: 10.1016/j.enconman.2015.09.068.
- [11] Q. Cao, W. Luan, and T. Wang, "Performance enhancement of heat pipes assisted thermoelectric generator for automobile exhaust heat recovery," *Appl. Therm. Eng.*, vol. 130, pp. 1472–1479, 2018, doi: 10.1016/j.applthermaleng.2017.09.134.
- [12] W. H. Chen, C. C. Wang, C. I. Hung, C. C. Yang, and R. C. Juang, "Modeling and simulation for the design of thermal-concentrated solar thermoelectric generator," *Energy*, vol. 64, pp. 287–297, 2014, doi: 10.1016/j.energy.2013.10.073.
- [13] E. Laux *et al.*, "Development of thermoelectric generator based on ionic liquids for high temperature applications," *Mater. Today Proc.*, vol. 5, no. 4, pp. 10195–10202, 2018, doi: 10.1016/j.matpr.2017.12.265.
- [14] L. Kütt, J. Millar, M. Lehtonen, and M. Märss, "Optimization of concentrated solar thermoelectric generator system for highest yearly electric output," *2015 56th Int. Sci. Conf. Power Electr. Eng. Riga Tech. Univ. RTUCON 2015*, pp. 3–8, 2015, doi: 10.1109/RTUCON.2015.7343170.
- [15] P. Huen and W. A. Daoud, "Advances in hybrid solar photovoltaic and thermoelectric generators," *Renew. Sustain. Energy Rev.*, vol. 72, no. October 2016, pp. 1295–1302,

- 2017, doi: 10.1016/j.rser.2016.10.042.
- [16] T. Y. Hwang, A. Y. Vorobyev, and C. Guo, “Enhanced efficiency of solar-driven thermoelectric generator with femtosecond laser-textured metals,” *Opt. Express*, vol. 19, no. S4, p. A824, 2011, doi: 10.1364/oe.19.00a824.
- [17] N. H. Thomas, Z. Chen, S. Fan, and A. J. Minnich, “Semiconductor-based Multilayer Selective Solar Absorber for Unconcentrated Solar Thermal Energy Conversion,” *Sci. Rep.*, vol. 7, no. 1, pp. 3–8, 2017, doi: 10.1038/s41598-017-05235-x.
- [18] S. O’halloran and M. M. Rodrigues, “AC 2012-3976: POWER AND EFFICIENCY MEASUREMENT IN A THERMOELECTRIC GENERATOR degrees in mechanical engineering from Kansas State University. Power and Efficiency Measurement in a Thermoelectric Generator,” no. 2000, 2000.
- [19] M. K. Rad, M. Omid, A. Rajabipour, F. Tajabadi, L. A. Rosendahl, and A. Rezaianakolaei, “Optimum thermal concentration of solar thermoelectric generators (STEG) in Realistic Meteorological Condition,” *Energies*, vol. 11, no. 9, 2018, doi: 10.3390/en11092425.
- [20] P. Li, L. Cai, P. Zhai, X. Tang, Q. Zhang, and M. Niino, “Design of a concentration solar thermoelectric generator,” *J. Electron. Mater.*, vol. 39, no. 9, pp. 1522–1530, 2010, doi: 10.1007/s11664-010-1279-0.
- [21] L. C. Ding, A. Akbarzadeh, and L. Tan, “A review of power generation with thermoelectric system and its alternative with solar ponds,” *Renew. Sustain. Energy Rev.*, vol. 81, no. August 2017, pp. 799–812, 2018, doi: 10.1016/j.rser.2017.08.010.
- [22] A. Date, A. Date, C. Dixon, and A. Akbarzadeh, “Theoretical and experimental study on heat pipe cooled thermoelectric generators with water heating using concentrated solar thermal energy,” *Sol. Energy*, vol. 105, pp. 656–668, 2014, doi: 10.1016/j.solener.2014.04.016.
- [23] M. S. Kim, M. K. Kim, S. E. Jo, C. Joo, and Y. J. Kim, “Refraction-Assisted Solar Thermoelectric Generator based on Phase-Change Lens,” *Sci. Rep.*, vol. 6, pp. 1–9, 2016, doi: 10.1038/srep27913.
- [24] L. L. Baranowski, G. J. Snyder, and E. S. Toberer, “Concentrated solar thermoelectric generators,” *Energy Environ. Sci.*, vol. 5, no. 10, pp. 9055–9067, 2012, doi: 10.1039/c2ee22248e.
- [25] S. Manikandan and S. C. Kaushik, “Thermodynamic studies and maximum power point tracking in thermoelectric generator-thermoelectric cooler combined system,” *Cryogenics (Guildf.)*, vol. 67, pp. 52–62, 2015, doi: 10.1016/j.cryogenics.2015.01.008.
- [26] S. Radkowski, K. Lubikowski, M. Wikary, and K. Szczurowski, “Seebeck phenomenon, calculation method comparison,” *J. Power Technol.*, vol. 95, pp. 63–67, 2015.
- [27] M. N. Zulkifli, I. Ilias, A. Abas, and W. M. W. Muhamad, “Finite element analysis on the thermoelectric generator for the waste heat recovery of solar application,” *AIP Conf. Proc.*, vol. 1877, 2017, doi: 10.1063/1.4999894.
- [28] R. Lamba, S. Manikandan, and S. C. Kaushik, “Performance Analysis and Optimization of Concentrating Solar Thermoelectric Generator,” *J. Electron. Mater.*, vol. 47, no. 9, pp. 5310–5320, 2018, doi: 10.1007/s11664-018-6410-7.
- [29] S. Manikandan and S. C. Kaushik, “Energy and exergy analysis of solar heat pipe based annular thermoelectric generator system,” *Sol. Energy*, vol. 135, pp. 569–577, 2016, doi:

- 10.1016/j.solener.2016.06.031.
- [30] K. S. Ong, “Review of solar, heat pipe and thermoelectric hybrid systems for power generation and heating,” *Int. J. Low-Carbon Technol.*, vol. 11, no. 4, pp. 460–465, 2016, doi: 10.1093/ijlct/ctv022.
- [31] T. H. Kil *et al.*, “A highly-efficient, concentrating-photovoltaic/thermoelectric hybrid generator,” *Nano Energy*, vol. 37, no. April, pp. 242–247, 2017, doi: 10.1016/j.nanoen.2017.05.023.
- [32] H. Xi, L. Luo, and G. Fraisse, “Development and applications of solar-based thermoelectric technologies,” *Renew. Sustain. Energy Rev.*, vol. 11, no. 5, pp. 923–936, 2007, doi: 10.1016/j.rser.2005.06.008.
- [33] O. H. Ando Junior, A. L. O. Maran, and N. C. Henao, “A review of the development and applications of thermoelectric microgenerators for energy harvesting,” *Renew. Sustain. Energy Rev.*, vol. 91, no. March, pp. 376–393, 2018, doi: 10.1016/j.rser.2018.03.052.
- [34] Y. Kishita, Y. Ohishi, M. Uwasu, M. Kuroda, H. Takeda, and K. Hara, “Evaluating the life cycle CO₂ emissions and costs of thermoelectric generators for passenger automobiles: A scenario analysis,” *J. Clean. Prod.*, vol. 126, pp. 607–619, 2016, doi: 10.1016/j.jclepro.2016.02.121.
- [35] S. Shanmugam, M. Eswaramoorthy, and A. R. Veerappan, “Modeling and analysis of a solar parabolic dish thermoelectric generator,” *Energy Sources, Part A Recover. Util. Environ. Eff.*, vol. 36, no. 14, pp. 1531–1539, 2014, doi: 10.1080/15567036.2011.555352.
- [36] C. Thornsberry, *Methicillin-resistant staphylococci*, vol. 9, no. 2. 1989.
- [37] G. A. Moore, “Modern Thermoelectrics,” *Electronics and Power*, vol. 30, no. 9. p. 733, 1984, doi: 10.1049/ep.1984.0389.
- [38] J. Chen, “Thermodynamic analysis of a solar-driven thermoelectric generator,” *J. Appl. Phys.*, vol. 79, no. 5, pp. 2717–2721, 1996, doi: 10.1063/1.361143.
- [39] H. B. Gao, G. H. Huang, H. J. Li, Z. G. Qu, and Y. J. Zhang, “Development of stove-powered thermoelectric generators: A review,” *Appl. Therm. Eng.*, vol. 96, pp. 297–310, 2016, doi: 10.1016/j.applthermaleng.2015.11.032.
- [40] R. Mal, R. Prasad, V. K. Vijay, and A. R. Verma, “The design, development and performance evaluation of thermoelectric generator (TEG) integrated forced draft biomass cookstove,” *Procedia Comput. Sci.*, vol. 52, no. 1, pp. 723–729, 2015, doi: 10.1016/j.procs.2015.05.085.
- [41] B. D. In, H. I. Kim, J. W. Son, and K. H. Lee, “The study of a thermoelectric generator with various thermal conditions of exhaust gas from a diesel engine,” *Int. J. Heat Mass Transf.*, vol. 86, pp. 667–680, 2015, doi: 10.1016/j.ijheatmasstransfer.2015.03.052.
- [42] B. Orr, A. Akbarzadeh, M. Mochizuki, and R. Singh, “A review of car waste heat recovery systems utilising thermoelectric generators and heat pipes,” *Appl. Therm. Eng.*, vol. 101, pp. 490–495, 2016, doi: 10.1016/j.applthermaleng.2015.10.081.
- [43] H. P. Garg, *Advances in Solar Energy Technology. Volume 1: Collection and Storage Systems*, vol. 1. 1987.
- [44] J. A. Duffie and W. A. Beckman, “Solar Engenierring of Thermal Process.” p. 893, 2006.

- [45] Verde, Giuseppe. "Thermal operating machine." *Int. J. Mech. Prod. Eng. Res. Dev* 7.5 (2017): 311-322.
- [46] Kumar, A. N. I. L., M. Chopkar, and A. Swarnakar. "Effect of Milling Time and Milling Media on the Formation of CrSi₂ from their Constituent Elements for Thermoelectric Materials." *Int. J. Metall. Mater. Sci. Eng* 5 (2015): 1-8.
- [47] Saleh, B., and M. S. Youssef. "Parametric analysis of an ejector refrigeration cycle activated by renewable energy." *International Journal of Mechanical and Production Engineering Research and Development (IJMPERD)* 9.3 (2019): 1143-1156.
- [48] Senthil, R. "Effect of secondary reflector on thermal performance of linear fresnel concentrated solar collector." *International Journal of Mechanical and Production Engineering Research and Development* 8.4 (2018).
- [49] Deshpande, Shripad V., and P. R. Devale. "Recent trends in using wireless sensor networks in industrial environment." *International Journal of Computer Networking Wireless and Mobile Communication (IJCNWMC)* 3 (2013): 11-20.
- [50] Kumar, Raja Ram, et al. "Design, control and experimental investigation of fault-tolerant five phase PMSG for wind power application." (2018).